The CRISPR Journal
Volume 5, Number 5, 2022
Mary Ann Liebert, Inc.
DOI: 10.1089/crispr.2022.0058

The CRISPR Journal

RESEARCH ARTICLE

Efficient Homology-Directed Repair with Circular Single-Stranded DNA Donors

Sukanya Iyer,[1,†] Aamir Mir,[2,†,‡] Joel Vega-Badillo,[2] Benjamin P. Roscoe,[1,§] Raed Ibraheim,[2,‡] Lihua Julie Zhu,[1,3] Jooyoung Lee,[2,**] Pengpeng Liu,[1] Kevin Luk,[1,††] Esther Mintzer,[1,***] Dongsheng Guo,[4] Josias Soares de Brito,[1] Charles P. Emerson Jr.,[4] Phillip D. Zamore,[2,5] Erik J. Sontheimer,[2,6,7,*] and Scot A. Wolfe[1,7,*]

Abstract

While genome editing has been revolutionized by the advent of CRISPR-based nucleases, difficulties in achieving efficient, nuclease-mediated, homology-directed repair (HDR) still limit many applications. Commonly used DNA donors such as plasmids suffer from low HDR efficiencies in many cell types, as well as integration at unintended sites. In contrast, single-stranded DNA (ssDNA) donors can produce efficient HDR with minimal off-target integration. In this study, we describe the use of ssDNA phage to efficiently and inexpensively produce long circular ssDNA (cssDNA) donors. These cssDNA donors serve as efficient HDR templates when used with Cas9 or Cas12a, with integration frequencies superior to linear ssDNA (lssDNA) donors. To evaluate the relative efficiencies of imprecise and precise repair for a suite of different Cas9 or Cas12a nucleases, we have developed a modified traffic light reporter (TLR) system (TLR-multi-Cas variant 1 [MCV1]) that permits side-by-side comparisons of different nuclease systems. We used this system to assess editing and HDR efficiencies of different nuclease platforms with distinct DNA donor types. We then extended the analysis of DNA donor types to evaluate efficiencies of fluorescent tag knockins at endogenous sites in HEK293T and K562 cells. Our results show that cssDNA templates produce efficient and robust insertion of reporter tags. Targeting efficiency is high, allowing production of biallelic integrants using cssDNA donors. cssDNA donors also outcompete lssDNA donors in template-driven repair at the target site. These data demonstrate that circular donors provide an efficient, cost-effective method to achieve knockins in mammalian cell lines.

Introduction

RNA-guided Cas9 and Cas12a proteins[1] have provided a facile tool for introducing targeted breaks within genomes. These double-strand breaks (DSBs) can be harnessed to engineer the genome through endogenous DNA repair pathways. Typically, DSBs are precisely repaired through the canonical nonhomologous end joining (c-NHEJ) pathway, restoring the original DNA sequence.[2] However, in the context of a programmable nuclease where DSB generation can reoccur, imprecise DNA repair may produce small insertions and deletions (indels) through c-NHEJ as well as alternative non homologous end joining (alt-NHEJ) pathways.[3] In contrast to the imprecise nature of these indels, the homology-directed repair (HDR) pathway results in precise rewriting of the genome in a template-dependent manner.[4–7] HDR is often utilized in the context of programmable nucleases to introduce specific changes to

[1]*Department of Molecular, Cell and Cancer Biology;* [2]*RNA Therapeutics Institute;* [3]*Program in Bioinformatics and Integrative Biology;* [4]*Wellstone Program, Department of Neurology;* [5]*Howard Hughes Medical Institute;* [6]*Program in Molecular Medicine; and* [7]*Li Weibo Institute for Rare Disease Research; University of Massachusetts Chan Medical School, Worcester, Massachusetts, USA.*
[†]*These two authors contributed equally to this work.*
[‡]Present address: Tessera Therapeutics, Somerville, Massachusetts, USA.
§Present address: Repertoire Immune Medicines, Cambridge, Massachusetts, USA.
**Present address: Vertex Pharmaceuticals, Boston, Massachusetts, USA.
***Present address: Harvard Medical School, Boston, MA.
[††]Present address: Excision BioTherapeutics, Cambridge, Massachusetts, USA.

*Address correspondence to: *Erik J. Sontheimer, RNA Therapeutics Institute, University of Massachusetts Chan Medical School, 364 Plantation Street, Worcester, MA 01605-2324, USA,* E-mail: erik.sontheimer@umassmed.edu *or Scot A. Wolfe, Department of Molecular, Cell and Cancer Biology, University of Massachusetts Chan Medical School, L.R.B. 619, 364 Plantation Street, Worcester, MA 01605, USA,* E-mail: scot.wolfe@umassmed.edu

the genome, such as adding fluorescent tags to proteins[8] or making a precise therapeutic correction to the desired locus.[9–11]

Given the broad utility of this technology for enabling precise insertions into mammalian genomes, several viral and nonviral approaches for the delivery of donor DNA into mammalian cells have been described.[12–16] The nature of the template used for HDR is dictated, in part, by the length of the desired genomic modification. For short insertions (<200 nt), single-stranded DNA (ssDNA) oligonucleotides harboring the mutation, as well as flanking homology arms that range from 35 to 60 nucleotides, are introduced into cells along with the Cas9 protein and guide-RNA.[13,17–19] When modifications longer than 200 bp are desired, double-stranded DNA (dsDNA) templates such as plasmids or polymerase chain reaction (PCR) products are typically used as donor templates.[20]

However, these double-stranded templates are often associated with high cellular toxicity and off-target integration events.[21] As an alternative to using dsDNA templates as donors for HDR, long ssDNA templates have been reported to have low cytotoxicity and high efficiencies of targeted integration at the site of interest.[22–24] Consequently, there is considerable interest in developing methods to generate long ssDNA templates to serve as donors for making targeted insertions in mammalian cells. Several recent examples include asymmetric PCR, commercial synthesis of long ssDNA (Genewiz, Inc.), ''Strandase'' enzyme-mediated removal of one strand of a linear dsDNA template (Catalog No. 632644; Takara Bio USA), use of pairs of nicking endonucleases followed by gel extraction of resulting ssDNA (Catalog No. DS615; Biodynamics Laboratory, Inc.), selective precipitation of a methanol-responsive polymer-tagged strand of a PCR amplicon under denaturing conditions, and reverse-transcription (RT)-based approaches to generate ssDNA.[22,23,25–28]

Most of these approaches require expensive and time-consuming purification steps to ensure complete removal of truncated ssDNA products. With RT-based approaches in particular, it is challenging to generate accurate ssDNA donors longer than 3–4 kb, especially in large molar quantities, because of the lack of proofreading activity and the limited processivity of reverse transcriptase enzymes.

As an alternative to these *in vitro* approaches, we explored the use of circular ssDNA (cssDNA) produced from phagemids as templates for HDR-mediated integration of DNA cassettes. Phagemid vectors have been used to generate ssDNA templates for site-directed mutagenesis,[29] DNA nanotechnology and DNA origami,[30] phage display technology for protein engineering,[31] and as templates for transcription in cell-free systems.[32] However, to our knowledge, their use as donors for achieving targeted integration of DNA in mammalian cells has not been evaluated.

In this study, we show that phagemid-derived cssDNA can be used to insert sequences efficiently and precisely in mammalian cells. We further compared HDR efficiencies obtained with phagemid-sourced cssDNA with those of linear ssDNAs (lssDNAs) generated using an RT-based method[23] and a streptavidin affinity purification approach with asymmetrically biotinylated PCR amplicons.[33] To this end, we used a redesigned traffic light reporter (TLR) system to evaluate HDR efficiencies for different forms of donor templates (plasmids, lssDNAs, and cssDNAs) in conjunction with SpyCas9 or three different Cas12a effectors delivered as ribonucleoproteins (RNPs) in HEK293T and K562 cells. We then compared knockin yields of lssDNA and cssDNA donor templates containing fluorescent reporter tags at four different endogenous sites in the human genome. Finally, we demonstrated the ability of cssDNA templates to create biallelic integration of a reporter cassette in different cell lines. Overall, our data show broad utility of cssDNA as donors for genome engineering applications.

Materials and Methods

Plasmids

All plasmids generated in this study were made using standard molecular biology techniques. A list of primers used to make the donor DNA templates are listed in Supplementary Table S1. A list of plasmids created is provided in Supplementary Table S2, and plasmids have been deposited in Addgene for distribution (Plasmid Nos. 87448, 107317, 117111, and 117405–117412).

Generation of ssDNA templates using phagemids

Preparation of cells. One milliliter of 2xYT media with 100 μg/mL of ampicillin was inoculated with a colony of XL1-blue cells transformed with the phagemid of interest. After culturing cells at 37°C for ~8 h or until the media became slightly cloudy (OD_{600} ~0.1), 50 μL of VCSM13 phage (10^{10-11} pfu/mL) was added to the bacterial culture and incubated without shaking at room temperature for 20 min. Cells were then transferred to 250 mL of 2xYT media with 100 μg/mL of ampicillin and cultured at 37°C for 1–2 h. To select for cells that had been infected by the phage, kanamycin was added to the cells to a final concentration of 75 μg/mL and cultured overnight.

Phage pellet preparation. Cells were pelleted from the media by centrifugation at 10,000 *g* for 20 min. The

supernatant containing phage was filtered through a vacuum filter (pore size 0.22 μm) to eliminate cell debris and remove any remaining bacterial cells from the supernatant. DNase I (Sigma) was added to a final concentration of 10 μg/mL and incubated at 37°C for 3 h to eliminate any remaining dsDNA contamination in the supernatant. Ten grams of PEG-8000 (Sigma) and 7.5 g of NaCl were added to 250 mL of supernatant and incubated at 4°C on ice for 1–2 h to precipitate the phage. The supernatant was spun at 12,000 *g* for 30 min at 4°C and the supernatant was carefully poured out and the phage pellet was retained. Care was taken to remove as much polyethylene glycol (PEG) solution from the bottle as possible by wiping the inner surface using Kimwipes.

DNA extraction. The ssDNA was extracted from the phage pellet using a modification of PureLink Midiprep columns from Life Technologies. The phage pellet was resuspended in 6 mL of 1 × Tris-EDTA (TE) buffer. Six milliliters of 4% sodium dodecyl sulfate (SDS) was added to the phage suspension and incubated at 70°C for 30 min. Six milliliters of buffer N3 or 3 M Potassium acetate (pH 5.5) was then added to the solution and spun at 12,000 *g* for 10 min at room temperature.

During this time, the PureLink Midiprep column was equilibrated by adding 10 mL of equilibration buffer. Following column equilibration, the supernatant containing cssDNA was applied to the column. The column was washed twice with 10 mL of wash solution and eluted using 5 mL of elution buffer. 3.5 mL of isopropanol or 12.5 mL of 100% ethanol was added to precipitate the DNA and incubated at −80°C for 2 h. The solution was spun at 12,000 *g* for 30 min to pellet the DNA. The DNA pellet was then washed with 5 mL of 70% ethanol and allowed to air-dry. The ssDNA was then resuspended in 50–100 μL of TE buffer and stored at −20°C. We typically obtain 100–200 μg of cssDNA from a 250 mL culture.

Generation of ssDNA templates using TGIRT

ssDNA donors were generated using reverse transcription of an RNA intermediate using TGIRT-III, as previously described.[23] Briefly, the donor sequence and its homology arms were cloned into a plasmid. Eight 50 μL PCRs were set up for each donor to amplify the cloned donor using forward primers that contain a 5′ overhang encoding the T7 promoter. The generated PCR products were pooled and purified using carboxylate-modified magnetic bead solution (#65152105050250; GE Healthcare). The purified DNA was used to generate the corresponding RNA by *in vitro* transcription (IVT) using HiScribe T7 polymerase (#E2040S; NEB). After purifying the RNA with carboxylate-modified magnetic beads, the reverse transcription reaction was generated using 400 pmol of RNA, 800 pmol of reverse transcription primer and 15 μL of 25 mM dNTP mix.

After annealing the primer at 65°C for 5 min, then on ice for 5 min, 3 μL of TGIRT-III enzyme (InGex) was added and the reaction incubated at 58°C for 3 h. The remaining RNA was hydrolyzed by base (0.5 M NaOH, 0.25 M EDTA [pH 8.0]) incubation at 95°C for 10 min. The sodium hydroxide (NaOH) was neutralized with an equal volume of 0.5 M HCl. The generated ssDNA donor was purified by carboxylate-modified magnetic beads and eluted with 20 or 15 μL of RNase-free water containing 2 mM Tris-HCl (pH 8.0).

Generation of ssDNA templates using biotin- and streptavidin-based affinity purification

The PCR product template for producing ssDNA was generated using one unmodified and one 5′-biotinylated primer (purchased from IDT). The High-Fidelity PCR product was purified by PCR clean-up gel extraction (QIAquick Gel Extraction Kit). Streptavidin magnetic Dynabeads (NanoLink™, Catalog No. M-1002; TriLink Biotechnologies, San Diego, CA) were washed and resuspended in binding solution (KilobaseBINDER™, Catalog No. 60101; Invitrogen, Life Technologies) as per the manufacturer's instructions and prepared for nucleic acid binding (17 μg of biotinylated dsDNA/mg Dynabeads, 0.8–3.3 kb). The prepared streptavidin-coated beads were incubated with a biotinylated PCR product for 3 h at room temperature or 4°C overnight while gently rotating the tubes to keep the beads in suspension.

The supernatant was collected in an Eppendorf tube and biotinylated DNA-coated beads were separated with a magnet for 4 min. The beads were washed twice with a buffer that consists of 50 mM Tris-HCl (pH 8.0), 2 M NaCl, and 0.05% Tween 20 by pipetting and using a volume equivalent to the solution used for nucleic acid binding, and then the tube was placed on the magnet for 2 min to collect the beads. The beads were then washed once with buffer containing 10 mM Tris-HCl (pH 8.0) and 50 mM NaCl. The bead-containing solution was then transferred to a fresh tube and the beads were separated from the solution using a magnet for 3 min.

Denaturation of dsDNA

Streptavidin beads bound to the biotinylated DNA were incubated with 155 μL of 0.1 N NaOH solution for 1 min at room temperature to achieve alkaline denaturation of the biotinylated and nonbiotinylated strands of the PCR product. Biotinylated ssDNA-coated beads were then separated with a magnet for 1 min. The supernatant was then

transferred to a new 1.5 mL tube and the tube was placed back on the magnetic stand for an additional 1 min. The solution containing the nonbiotinylated strand was immediately neutralized by the addition of 1 M glacial acetic acid (15 μL of 1 M glacial acetic acid to neutralize 150 μL of 0.1 N NaOH), and an equal volume of 10 mM Tris-HCl (pH 7.5) solution was then added. The sample was applied on a Spin-X centrifuge tube filter (0.22 μm cellulose acetate) to remove any beads ($\sim$0.85 μm) and transferred to a fresh tube.

The nonbiotinylated strand was precipitated using ethanol precipitation and then redissolved in water.

Circularization of lssDNA

To circularize lssDNA donors generated by PCR using one 5′-phosphorylated and one 5′-biotinylated primer (IDT), the nonbiotinylated and phosphorylated ssDNA was generated by the affinity purification method described above. Subsequently, phosphorylated ssDNA (e.g., $\sim$20 pmol) was annealed with a 1.2-fold molar excess of splint oligonucleotide (24 pmol) that spans the two ends of the ssDNA in 1 × *Escherichia coli* DNA ligase buffer solution (NEB) to a final volume of 200 μL by heating the solution to 95°C for 2 min and then cooling the reaction on ice for 2 min.

After annealing, 40 units of *E. coli* DNA ligase (NEB) was added to the solution and incubated at 45°C for 1 h to allow ligation of the ssDNA ends to proceed to completion. The solution was then treated with 40 units of exonuclease I (NEB) and 40 units of exonuclease III (NEB) and incubated at 37°C for 30 min to eliminate lssDNA. Exonucleases were inactivated at 70°C for 20 min. The cssDNA was cleaned by a NucleoSpin® (Macherey-Nagel GmbH & Co. KG, Düren, Germany) column, concentrated using ethanol precipitation, and then redissolved in water. DNA fractions were then run on a denaturing agarose gel (2%, 70 V, 2 h) to examine the integrity and purity of the cssDNA.

Cell culture

HEK293T cells were maintained in Dulbecco's modified Eagle's medium supplemented with 10% fetal bovine serum (FBS) and 1% penicillin and streptomycin (Gibco). K562 cells were maintained in RPMI 1650 media with 1 mM glutamine supplemented with 10% FBS and penicillin and streptomycin. All the cells were maintained in a humidified incubator at 37°C and 5% CO_2.

Electroporation of Cas9 or Cas12a RNPs

All electroporations were done using the Neon transfection system (Invitrogen). Twenty picomole of SpyCas9-3xNLS, AspCas12a, LbaCas12a, or FnoCas12a protein, along with 25 pmol of sgRNA (for SpyCas9) or 60 pmol of crRNA (for Cas12a), was added per reaction. Guide RNA was either generated using IVT (TLR-multi-Cas variant 1 [TLR-MCV1] locus) or was purchased from Synthego (for SpyCas9 sgRNAs targeting endogenous loci). RNPs and guide-RNAs were precomplexed in buffer R for 10–20 min at room temperature and the solution was made up to a final volume of 12 μL. For electroporating K562 cells, 150,000–200,000 cells per reaction were used. Cells for a reaction were spun down and the media were carefully removed. Cells were resuspended in 10 μL of buffer R containing the desired nuclease and nucleofected with 3 pulses of 1600 V for 10 ms using a 10 μL Neon Tip.

Cells were then plated in 24-well plates into 500 μL of RPMI 1650 media supplemented with 10% FBS and cultured in a humidified incubator at 37°C and 5% CO_2 for 3–4 days for TLR experiments, and for 2 weeks for experiments with donors to knock in fluorescence tags at endogenous sites, before analysis of samples using flow cytometry. For all HDR experiments except those in Figure 2C, 1 pmol of cssDNA, lssDNA, or plasmid donor DNA was used. Donor DNA was added to the cells resuspended in buffer R or buffer R containing Cas9/Cas12a RNP.

For experiments with HEK293T cells, roughly 100,000 cells per reaction were used and the cells were given 2 pulses of 1100 V for 20 ms. For experiments shown in Figure 1B and 2B, 3 pmols of cssDNA, lssDNA, or plasmid donor DNA was used. For the rest of the experiments except those in Figure 2C, 1 pmol of donor DNA was used for the HDR experiments.

Flow cytometry analysis

Cells were first washed twice with 1 × phosphate-buffered saline before analysis using flow cytometry. All the flow cytometry was performed on MACSQuant VYB by Miltenyi. For detection of mCherry signal, a yellow laser (wavelength 561 nm) was used for excitation and a 615/20 nm emission filter was used. To detect the green fluorescent protein (GFP) signal, a blue laser (excitation wavelength 488 nm and emission filter 525/50 nm) was used. Twenty thousand events were recorded for each sample and the data were analyzed using FlowJo V.9.0 software. Cells were first gated on forward scatter (FSC)-A and side scatter-A plots to remove cell debris. This population was further plotted on an FSC-A versus FSC-H plot to circumscribe the single-cell population. Finally, a bivariate plot between FITC-A and txRED signal was used to estimate the percentage of GFP-positive or mCherry-positive populations and was reported in this study as a measure of gene editing or homologous recombination as applicable.

TIDE analysis

Genomic DNA was extracted from mammalian cells using the Sigma GenElute kit or the Qiagen DNeasy Blood & Tissue Kits. PCRs were performed using genomic DNA as template, with primers listed in Supplementary Table S1 as per the manufacturer's directions. Subsequently, PCR product was purified using the Zymo DNA purification kit and sent for analysis by Sanger sequencing along with primers listed in Supplementary Table S1. The chromatograms were analyzed with the TIDE analysis web tool (https://tide.nki.nl/).[34]

Cas9 and Cas12a purification

Protein purification for the 3xNLS-SpyCas9 and Cas12a-2xNLS proteins followed a common protocol as previously described.[35] The generation and characterization of the 3xNLS-SpyCas9 and LbaCas12a-2xNLS constructs have been recently described.[36–38] The pET21a plasmid backbone (Novagen) was used to drive the expression of a hexa-His-tagged version of each protein. The plasmid expressing 3xNLS-SpyCas9 (or each Cas12a-2xNLS) was transformed into *E. coli* Rosetta (DE3) pLysS cells (EMD Millipore) for protein production. Cells were grown at 37°C to an OD_{600} of ~0.2, then shifted to 18°C, and induced at an OD_{600} of ~0.4 for 16 h with IPTG (1 mM final concentration). Following induction, cells were pelleted by centrifugation and then resuspended with Ni^{2+}-NTA buffer (20 mM Tris-HCl [pH 7.5] + 1 M NaCl +20 mM imidazole +1 mM TCEP) supplemented with HALT Protease Inhibitor Cocktail, EDTA-Free (100×; Thermo Fisher), and lysed with an M-110s Microfluidizer (Microfluidics) following the manufacturer's instructions.

The protein was purified from the cell lysate using Ni^{2+}-NTA resin, washed with five volumes of Ni^{2+}-NTA buffer, and then eluted with an elution buffer (20 mM Tris-HCl [pH 7.5], 500 mM NaCl, 500 mM imidazole, and 10% glycerol). The 3xNLS-SpyCas9 (or each

FIG. 1. Comparisons of the integration efficiencies of different donor topologies on HDR using the TLR-MCV1 cassette in human cells. **(A)** The schematic depicts the TLR-MCV1 system showing the SFFV promoter driving the expression of GFP and mCherry, separated by a ribosome-skipping T2A signal. The yellow arrow depicts the SFFV promoter driving the expression of the GFP-T2A-mCherry cassette. The orange box indicates the insertion disrupting GFP containing target sequences for different Cas effectors. The sequence of insertion is shown below the schematic of TLR-MCV1. Sequences and arrows in blue indicate overlapping PAMs and a common cut site associated with SpyCas9, Nme1Cas9, CjeCas9, and SauCas9. The bolded black sequence and black arrow depict the Nme2Cas9 PAM and cut site, respectively. The magenta text shows PAMs associated with Cas12a effectors, and their approximate cut sites are shown by magenta lines. The PAMs associated with Geo1Cas9 and Geo2Cas9 are highlighted in green italicized text and brown-underlined italicized text, respectively. The cut sites for these two Cas9s are shown by green and brown arrows, respectively. DSBs at any of the sites may be imprecisely repaired through the NHEJ pathway resulting in mCherry expression (shown on the left) if repair results in productive translation due to a +1 frameshift. In the presence of donor DNA, HDR-mediated correction of the "broken" GFP region results in restoration of GFP expression (shown on the right). **(B)** Efficacy of distinct DNA templates in driving HDR. The graph depicts the percentage of GFP-positive cells obtained after codelivery of SpyCas9 or AspCas12a RNP with cssDNA, T-lssDNA, B-lssDNA, or plasmid DNA repair templates into TLR-MCV1 K562 cells (upper gray box) and TLR-MCV1 HEK293T cells (lower blue box). Bars represent the mean from three independent biological replicates and error bars represent the s.e.m. **(C)** Schematic of the approach used to generate circularized B-lssDNA. A short oligonucleotide (red) is hybridized to the B-lssDNA containing a 5′-phosphorylated end such that the oligo spans the 5′ and 3′ ends of the lssDNA. The sample is treated with *Escherichia coli* DNA ligase to ligate the ends. The lssDNA sample is then treated with exonucleases (I and III) to eliminate residual uncircularized lssDNA. The native agarose gel shows linear and ligated lssDNA before and after treatment with exonucleases, which digest unprotected, linear DNA species. **(D)** The graphs depict the percentage of GFP-positive cells obtained after codelivery of SpyCas9 with B-lssDNA and circularized B-lssDNA DNA repair templates into TLR-MCV1 K562 cells (upper gray box) and TLR-MCV1 HEK293T cells (lower blue box). Bars represent the mean from three independent biological replicates and error bars represent (s.e.m.). n.s., p value not significant; ***$p < 0.001$. B-lssDNA, biotin-based affinity purified linear ssDNA; cssDNA, circular ssDNA; DSB, double-strand break; GFP, green fluorescent protein; HDR, homology-directed repair; lssDNA, linear ssDNA; NHEJ, nonhomologous end joining; PAM, protospacer adjacent motif; RNP, ribonucleoprotein; s.e.m., standard error of the mean; ssDNA, single-stranded DNA; TLR-MCV1, traffic light reporter multi-Cas variant 1; T-lssDNA, reverse-transcription generated linear ssDNA.

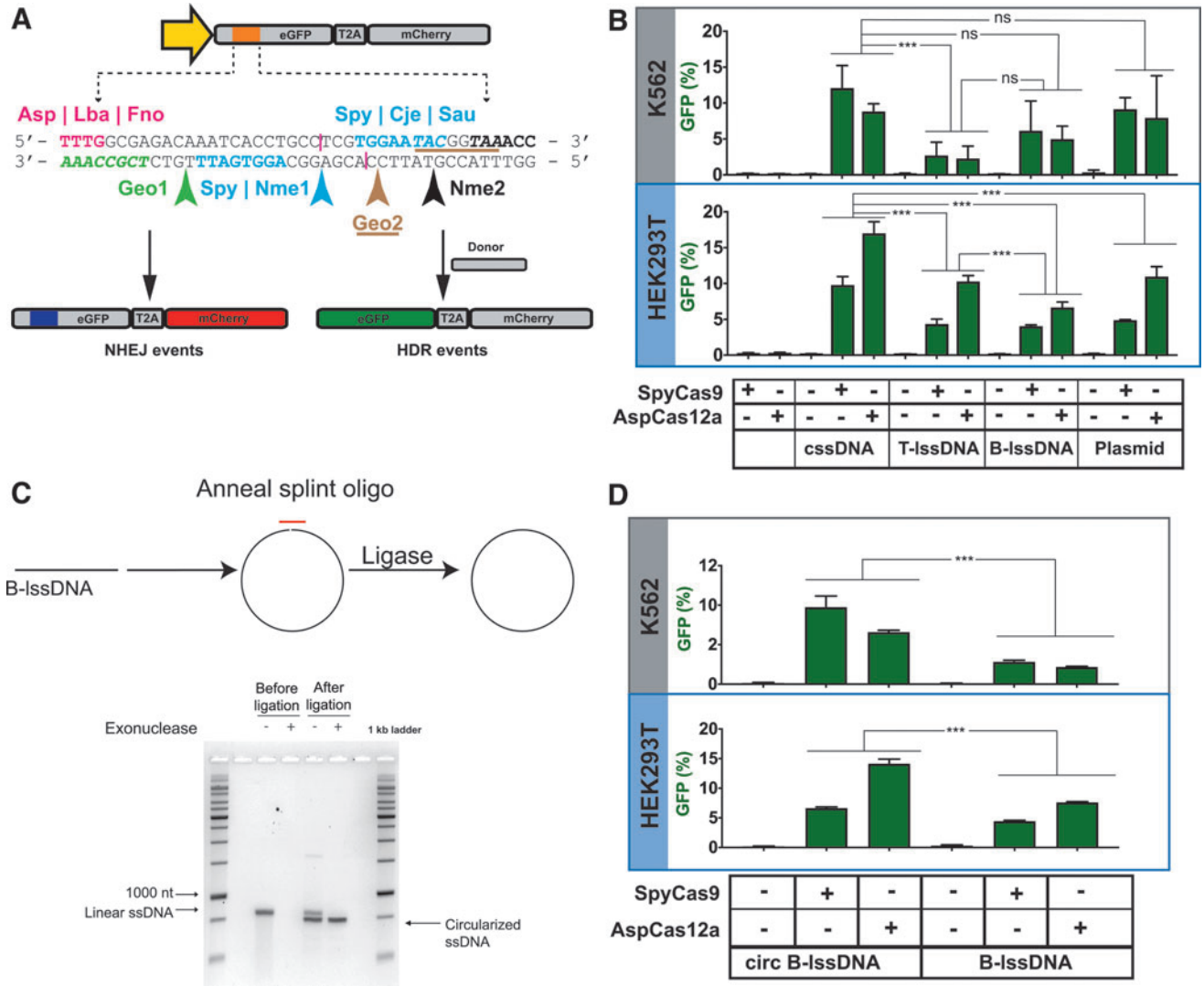

Cas12a) protein was dialyzed overnight at 4°C in 20 mM HEPES-NaOH (pH 7.5), 500 mM NaCl, 1 mM EDTA, and 10% glycerol. Subsequently, the protein was step-dialyzed from 500 mM NaCl to 200 mM NaCl (final dialysis buffer: 20 mM HEPES-NaOH [pH 7.5], 200 mM NaCl, 1 mM EDTA, and 10% glycerol).

Next, the protein was purified by cation exchange chromatography (column = 5 mL HiTrap-S; buffer A = 20 mM HEPES-NaOH [pH 7.5] + 1 mM TCEP; buffer B = 20 mM HEPES-NaOH [pH 7.5] + 1 M NaCl +1 mM TCEP; flow rate = 5 mL/min; column volume = 5 mL) followed by size-exclusion chromatography (SEC) on a Superdex-200 (16/60) column (isocratic size-exclusion running buffer = 20 mM HEPES-NaOH [pH 7.5], 150 mM NaCl, 1 mM TCEP for 3xNLS-SpyCas9; or 20 mM HEPES-NaOH [pH 7.5], 300 mM NaCl, 1 mM TCEP for each Cas12a-2xNLS). The primary protein peak from the SEC was concentrated in an Ultra-15 Centrifugal Filter Ultracel-30K (Amicon) to a concentration around 100 μM based on absorbance at 280 nm.

The purified protein quality was assessed by SDS–polyacrylamide gel electrophoresis (SDS-PAGE)/Coomassie staining to be >95% pure, and the protein concentration was quantified with the Pierce™ BCA Protein Assay Kit (Thermo Fisher Scientific). Protein was stored at −80°C until further use.

In vitro transcription

The DNA cassette containing the U6 promoter and the sgRNA framework for SpyCas9 was cloned from pLKO1-puro vector into pBluescript SK II+ backbone.[37] Plasmids expressing each guide RNA from the U6 promoter were constructed by annealing oligonucleotides encoding guide-RNA and cloning it into BfuAI cleavage sites in this vector (Guide sequences

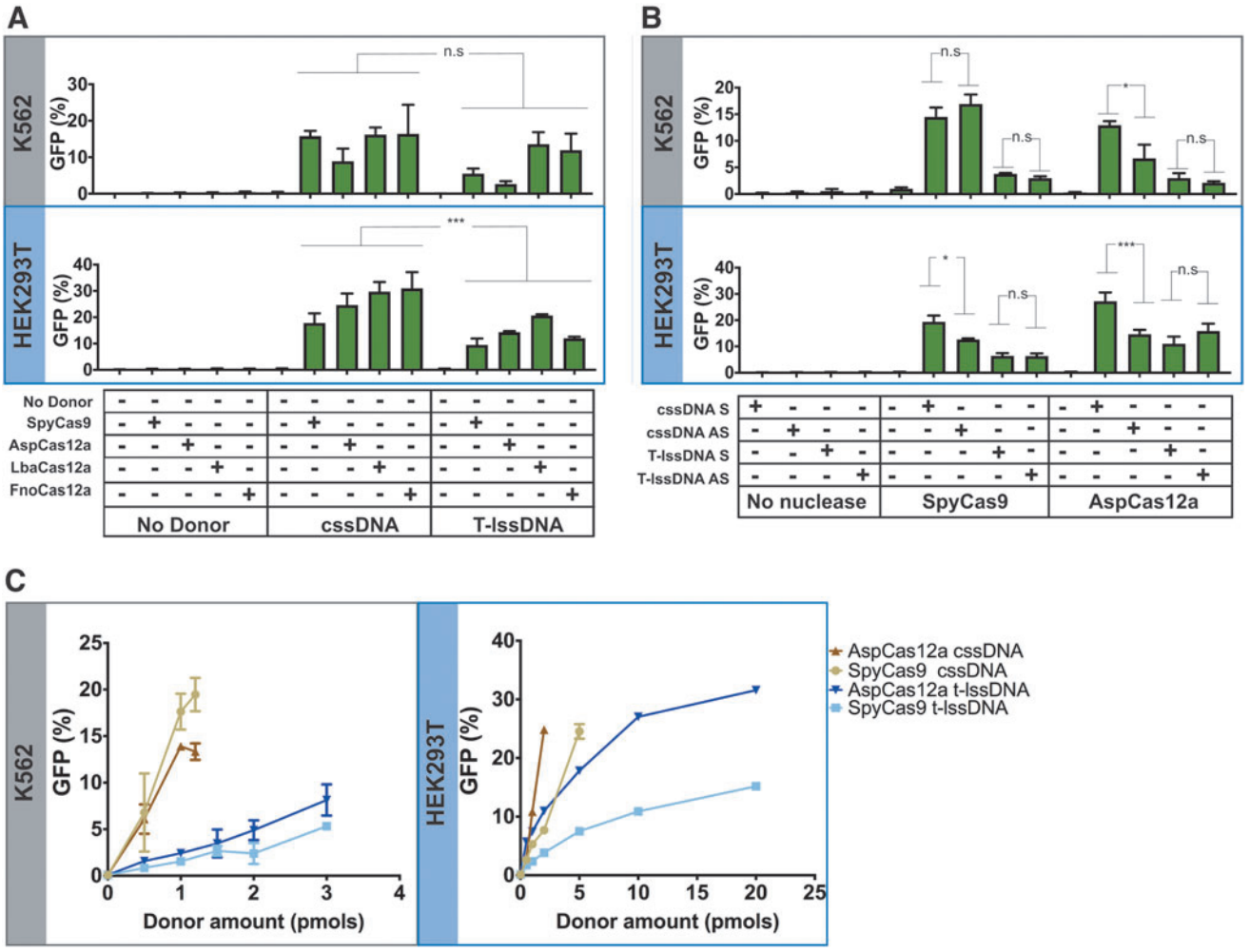

FIG. 2. Characterization of the HDR efficiencies of cssDNA and T-lssDNA. **(A)** Comparison of cssDNA- and T-lssDNA-mediated HDR efficiency upon treatment of TLR-MCV1 cells with distinct Cas effectors. The graphs depict the percentage of GFP-positive cells obtained after codelivery of SpyCas9, AspCas12a, LbaCas12a, or FnoCas12a with cssDNA and T-lssDNA DNA repair templates into TLR-MCV1 K562 cells (upper gray box) and TLR-MCV1 HEK293T cells (lower blue box). Bars represent the mean from three independent biological replicates and error bars represent the s.e.m. **(B)** Effect of cssDNA and T-lssDNA donor orientation on HDR efficiency. The graphs depict the percentage of GFP-positive cells obtained after codelivery of SpyCas9 or AspCas12a (targeting the same strand) with sense (S) and antisense (AS) strand cssDNA and T-lssDNA, DNA repair templates into TLR-MCV1 K562 cells (upper gray box) and TLR-MCV1 HEK293T cells (lower blue box). Bars represent the mean from three independent biological replicates for K562 cells and six independent replicates for HEK293T cells. Error bars represent s.e.m. **(C)** Dose dependence of cssDNA and T-lssDNA donor template-mediated HDR efficiency. The graphs depict the percentage of GFP-positive cells as a function of increasing cssDNA and T-lssDNA donor DNA in the presence of SpyCas9 and AspCas12a proteins in TLR-MCV1 K562 cells (left) and HEK293T cells (right). Points represent the mean from three independent biological replicates, and error bars represent s.e.m. n.s., p value not significant; *$p < 0.05$; ***$p < 0.001$.

in Supplementary Table S3). IVT DNA templates for SpCas9 guides were amplified from the cognate plasmids using NEB Q5 High-Fidelity DNA Polymerase for 30 cycles (98°C, 15 s; 65°C, 25 s; 72°C, 20 s), using primer sets designed to include the T7 scaffold (Supplementary Table S1). For crRNA generation for Cas12a orthologs, templates for IVT were generated by PCR amplification of oligonucleotides designed to include the T7 scaffold along with the guide-RNA and a 15-mer overlap sequence to allow annealing between

the oligos (Supplementary Table S1). The oligonucleotides encoded the full-length direct repeat crRNA sequence.[37]

Thirty cycles of amplification were conducted using NEB Q5 High-Fidelity DNA polymerase (98°C, 15 s; 60°C, 25 s; 72°C, 20 s). The PCR products were purified using the Zymo DNA Clean & Concentrator Kit (Cat. #D4005; Zymo). IVT reactions were performed using the HiScribe T7 High Yield RNA Synthesis Kit using 300 ng of PCR product as template (Cat. #E2040S; NEB). After incubation for 16 h at 37°C, samples were treated with DNase I for 40 min at 37°C to remove any DNA contamination. Each guide-RNA was purified using the Zymo RNA Clean and Concentrator Kit. The final RNA concentration was measured using a NanoDrop instrument and stored at −80°C until further use.

Statistical analysis

R, a system for statistical computation and graphics, was used for the analysis.[39] The percentage of knockin was first arcsin-transformed to homogenize the variance. Levene's test indicates that the assumption of homogeneity of variances was met. For Figure 3 and data plotted in Supplementary Figure S8, a three-way analysis of variance (ANOVA) with a completely randomized design was performed to test whether there were main effects of DNA topology, target gene, and fluorescent tag, and whether there was a gene- or/and fluorescent tag-dependent topology effect. Otherwise, two levels of topology were compared within each combination of genetic loci and fluorescent tag under the ANOVA framework using the lsmeans package[40] if there was a significant difference among different treatments (F-test $p < 0.01$). For Figure 2B, the three primary factors considered were DNA topology, Cas type, and orientation.

For the other figures, two-way ANOVA with completely randomized design was performed to test whether there was an overall difference among the different treatment groups. When the F-test was significant ($p < 0.01$), predefined contrasts were performed within the ANOVA framework using the lsmeans package. p Values were adjusted using the Hochberg method to correct for multiple inferences.[41]

Results

Generating lssDNA and cssDNA templates for HDR in mammalian cells

To address the challenges associated with long ssDNA donor production, we investigated a number of different approaches for generating ssDNA donors, as well as the relative efficiencies of HDR when using the resulting ssDNA products. While most efforts to generate ssDNA donors have focused on linear molecules, we explored the properties of cssDNAs as donors for HDR. Phagemids are chimeric vectors that contain plasmid and bacteriophage origins of replication. Upon superinfection of the host bacteria with helper phage to supply the phage DNA replication machinery, one strand of the phagemid vector is packaged into bacteriophage particles and extruded into the media from whence cssDNA can be purified (Supplementary Fig. S1A).[42] Although a standard protocol to purify ssDNA from phagemids yielded reasonable quantities of DNA, we observed the presence of contaminating *E. coli* genomic DNA in the ssDNA preparation, as reported previously.[43]

To remove contaminating *E. coli* genomic DNA in preparation for donor DNA transfection into mammalian cells, we modified a purification protocol described by Vieira and Messing,[44] where we incorporated a DNase I digestion step before bacteriophage uncoating and subsequently purified the cssDNA using an anion exchange column.

To provide a benchmark for aspects of donor DNA production and direct comparison of HDR rates in mammalian cells, we also evaluated two methods for generating lssDNA templates. First, lssDNA was generated using a published reverse transcription (RT) method (T-lssDNA) in which cDNA is generated by a processive reverse transcriptase such as TGIRT-III.[16] RT-based approaches (Supplementary Fig. S1B) can be effective for generating ssDNA donors up to 3.5 kb in length.[22,23,45,46] However, the reverse transcriptase enzymes used for generating lssDNA generally lack proofreading activity,[47] which makes the fidelity of the resulting template a concern.[27] In addition, these enzymes often generate truncated ssDNA products, as well as the desired full-length ssDNA products. Truncated products are particularly prevalent for templates with stable secondary structure elements necessitating further size-based purification before use in HDR experiments (Supplementary Fig. S2A and Supplementary Table S4).[48]

As an alternative to RT-based methods, we reasoned that ssDNA templates generated from asymmetrically biotinylated PCR products would produce longer ssDNA templates with higher sequence fidelity. Accordingly, we utilized an approach to generate ssDNA templates using biotin-based affinity purification of ssDNA (B-lssDNA) by exploiting the biotin–streptavidin interaction.[49] In this method, one PCR primer used for donor amplification is biotinylated, which allows the resulting PCR product to be strand-specifically bound to streptavidin-coated beads. Subsequently, the DNA strands are separated by alkaline denaturation and the nonbiotinylated strand is isolated and used as a donor for HDR (Supplementary Fig. S1C). ssDNA templates generated by all these methods were treated with S1 nuclease to confirm the single-stranded nature of the templates generated (Supplementary Fig. S2B).

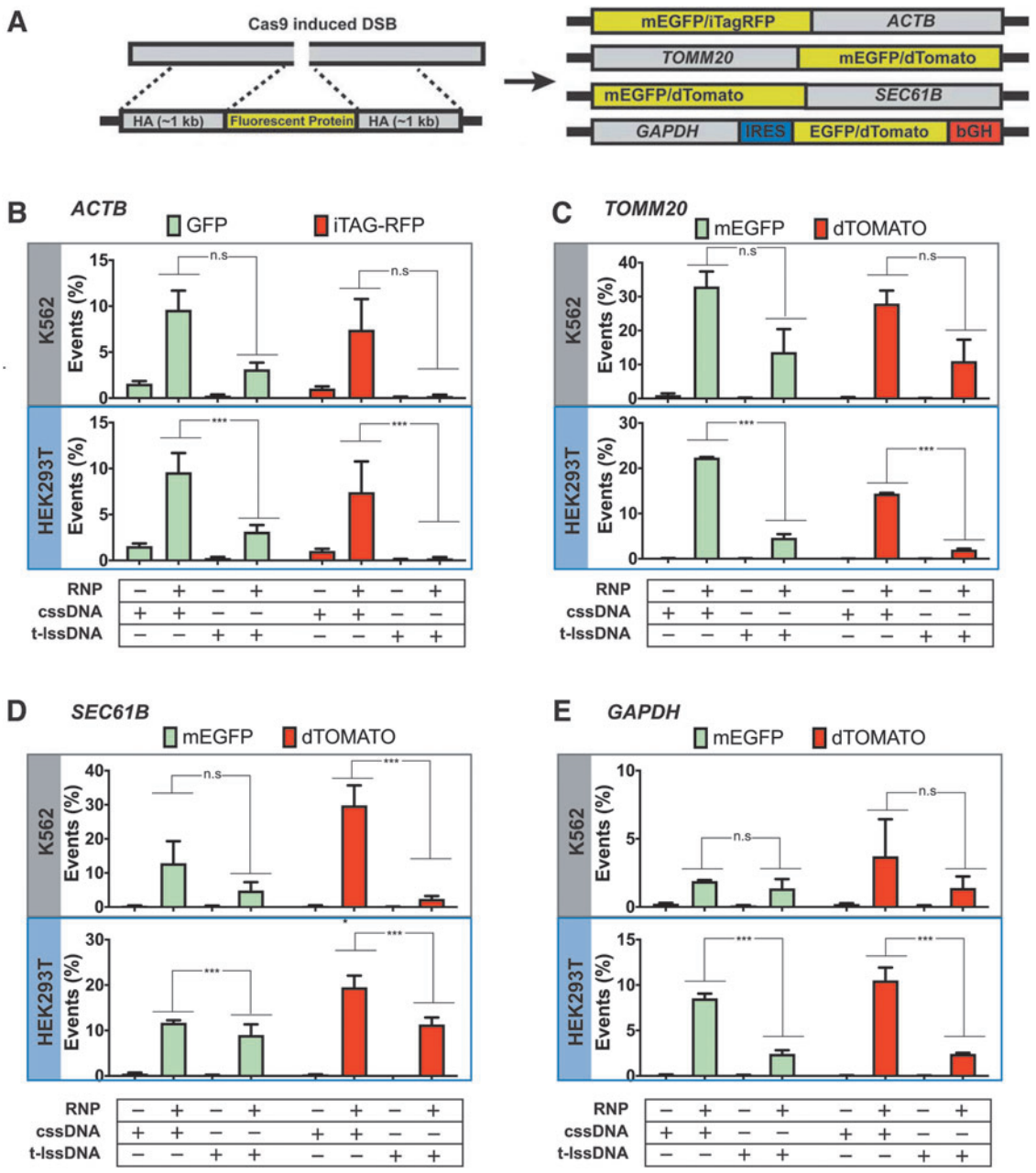

FIG. 3. Comparison of the type of DNA donor on the efficiency of HDR at endogenous genomic loci in human cells. **(A)** Schematic of fluorescent protein tagging. The left panel shows a schematic of a genomic region containing the SpyCas9 target site and the design of a donor template containing the fluorescent protein of interest flanked by HA. The right panel shows a schematic of each target genomic locus and the arrangement of the fluorescent tag (EGFP, dTomato, or iTag-RFP) following integration. Three of the donors (targeting *ACTB*, *TOMM20*, and *SEC61B*) produce direct fusions of the tag to the endogenous protein. The donor designed to fluorescently tag the *GAPDH* locus contains an IRES and a bGH polyadenylation sequence. **(B–E)** Bar graphs displaying the percentages of fluorescent cells obtained upon codelivery of 20 pmoles of SpyCas9 complexed with 25 pmoles of guide-RNA targeting the **(B)** *ACTB*, **(C)** *TOMM20*, **(D)** *SEC61B*, or **(E)** *GAPDH* locus with or without cssDNA or T-lssDNA as a donor template. Bars represent the mean from three independent biological replicates and error bars represent s.e.m. n.s.: p value not significant; ***$p < 0.001$. bGH, bovine growth hormone; EGPF, enhanced green fluorescence protein; GAPDH, glyceraldehyde 3-phophate dehydrogenase; HA, homology arms; IRES, internal ribosome entry site; RFP, red fluorescent protein.

While the cssDNA template was completely digested by the addition of S1 nuclease, we detected undigested species upon digestion of both T-lssDNA and B-lssDNA.

Consequently, we performed Sanger sequencing on equivalent ssDNA templates and plasmids using a primer that should not hybridize to the recovered ssDNA strand to detect trace amounts of the complementary strand. We detected small amounts of the complementary strand (implying the presence of dsDNA) for both T-lssDNA and B-lssDNA, but not for the cssDNA (Supplementary Fig. S2C). While all three approaches yielded ssDNA up to at least 3300 bases in length, the phagemid-based approach proved to be most economical while also generating large quantities of full-length ssDNA with the highest strand purity for use as HDR templates (Table 1).

TLR-MCV1: a system to evaluate genome-editing efficiency by multiple nucleases

Previously, Certo et al described a TLR system that provides positive fluorescence readouts for both error-prone DSB repair and precise HDR.[50] It consists of a tandem expression cassette consisting of a ''broken'' GFP coding sequence followed by an out-of-frame mCherry cassette (Fig. 1A). The GFP sequence is disrupted by an insertion harboring various nuclease target sites to initiate DSB formation. DSB repair by pathways such as NHEJ can result in indels that place the downstream mCherry coding sequence in frame for productive translation (+1 frameshift). In addition, precise HDR of the locus can be evaluated by codelivering a truncated GFP donor repair template with a nuclease, which will restore GFP expression while leaving the mCherry coding sequence out of frame. The fraction of GFP- and mCherry-positive cells can be rapidly measured using flow cytometry to determine editing outcomes as a function of the nuclease and donor DNA composition.

We redesigned the original TLR to incorporate target sites for several currently characterized nucleases (Fig. 1A) by introducing protospacer adjacent motifs (PAMs) belonging to Cas9/Cas12a orthologs from *Streptococcus pyogenes* (SpyCas9),[51,52] *Neisseria meningitidis* (Nme1Cas9 and Nme2Cas9),[53–55] *Campylobacter jejuni* (CjeCas9),[56–58] *Staphylococcus aureus* (SauCas9),[59] *Geobacillus stearothermophilus* (GeoCas9),[60] Lachnospiraceae bacterium ND2006 (LbaCas12a),[61] *Acidaminococcus* sp. (AspCas12a),[61] and *Francisella novicida* (FnoCas12).[62] For several of the Cas9 orthologs (SpyCas9, Nme1Cas9, CjeCas9, and SauCas9), DSB formation can be targeted to the exact same position. We also incorporated a second SpyCas9 target site on the opposite strand such that both SpyCas9 target sites will produce a DSB at the same position. Similarly, the Cas12a orthologs have overlapping PAMs in the incorporated target site and therefore will generate staggered cuts within the same region.

All of these target sites were combined into a sequence framework that lacks stop codons in the +1 reading frame to enable mCherry expression following the induction of a suitable indel. Hence, our updated reporter (TLR-MCV1) provides a useful platform for direct comparison of genome editing properties of the major RNA-guided genome editing tools described to date.

A single copy of TLR-MCV1 was introduced into HEK293T and K562 cells by lentiviral transduction. Using plasmid transfections of HEK293T cells to introduce the nucleases, guide-RNA (listed in Supplementary Table S3), and a plasmid donor template (pCVL-SFFV-d14GFP-Donor), we observed that all the Cas9/Cas12a sites can be targeted by the cognate nucleases to induce precise and imprecise genome editing in mammalian cells (Supplementary Fig. S3). The two GeoCas9-expressing plasmids produced inefficient editing, which may be due to suboptimal codon usage, or due to GeoCas9's preference for higher temperatures, or both.[60]

cssDNA donors outperform lssDNA donors for HDR

The TLR-MCV1 provides an ideal system for direct comparisons of different DNA donor architectures since both the NHEJ and HDR efficiencies can be measured using different Cas nucleases at the same locus. To create DSBs in cells, delivery of Cas9 or Cas12a RNPs has gained favor because these complexes can be readily electroporated into a wide variety of cell types.[36,63–65] Furthermore, due to their rapid turnover in cells, Cas9/

Table 1. Features of different single-stranded DNA preparation methods

Preparation method	*Typical yield/prep, μg*	*Cost/prep*	*Time/prep*	*Maximum length of ssDNA prepared, kb*
cssDNA	100–200	$14	24 h for expression; 6 h for purification	13
T-lssDNA	9	$65	11 h for purification	3.5
B-lssDNA	12	$109	9 h for purification	3.3

cssDNA, circular ssDNA; B-lssDNA, biotin-based affinity purified linear ssDNA; ssDNA, single-stranded DNA; T-lssDNA, reverse-transcription generated linear ssDNA.

Cas12a RNPs display lower off-target activity than other delivery modalities without compromising on-target editing activity, thereby significantly improving the specificity of targeted genomic modifications.[64,66] Delivery of SpyCas9 protein complexed with its guide-RNA (SpyCas9 RNPs), or each of the three Cas12a orthologs as RNPs, proved highly effective at editing the reporter,TLR-MCV1, with indel efficiencies >70% achieved as measured by TIDE (Supplementary Fig. S4).[34]

Next, we tested different types of ssDNA donors or a plasmid donor with SpyCas9 and AspCas12a RNPs. As shown in Figure 1B and Supplementary Figure S5A, cssDNA elicited higher HDR efficiencies relative to equimolar quantities of lssDNA donors or the plasmid donor in both K562 and HEK293T cells. Using cssDNA, we achieved a statistically significant approximately twofold increase in HDR yields compared with lssDNA (Supplementary Table S5). This was true for both SpyCas9- and AspCas12a-based editing. CssDNA also achieved higher GFP integration efficiencies in comparison with plasmid donors in both K562 and HEK293T cells. Notably, we did not observe a significant difference between T-lssDNA and B-lssDNA donor efficiency in K562 cells ($p = 0.0797$), indicating that lssDNAs generated using two different approaches were largely indistinguishable once generated and purified (Supplementary Table S5).

There was a statistically significant difference ($p = 0.03$) between T-lssDNA and B-lssDNA when tested in HEK293T cells with AspCas12a. However, the increase shown by T-lssDNA relative to B-lssDNA is modest (<4%). Overall, among the different forms of DNA templates tested, cssDNA realized the highest HDR efficiencies.

The improved efficiency of knockin using cssDNA may be due to the increased exonuclease protection afforded by the circular nature of the ssDNA. To test this hypothesis, we circularized the lssDNA by splint-mediated ligation and tested this circularized form in TLR-MCV1 cells (Fig. 1C). Circularization of lssDNA resulted in significant ($p < 0.0001$) enhancement of HDR relative to the unligated precursor in both the cell lines (Fig. 1D and Supplementary Fig. S5B and Supplementary Table S5) and comparable efficiencies with those observed with phagemid-derived cssDNA donors. This is consistent with previous studies that demonstrated improved function of end-protected nucleic acids in various cell types.[67]

Cas12a nucleases produce superior HDR yields at the TLR-MCV1 locus

Cas12a-based genome editing has been reported to achieve higher rates of HDR, relative to SpyCas9, since it generates 5′ overhangs and more rapidly releases the PAM-distal DNA end following cleavage.[68] To explore this possibility further, we tested different orthologs of Cas12a with lssDNA and cssDNA donors. Since we previously did not observe substantial difference between B-lssDNA and T-lssDNA in HDR efficiency at the TLR-MCV1 locus, we only included T-lssDNA for the subsequent comparisons in TLR-MCV1-related experiments. As shown in Figure 2A, the general trends for cssDNA and T-lssDNA held consistent across all the tested nucleases. In HEK293T cells, cssDNA collectively showed significantly higher HDR rates than T-lssDNA molecules for all the nucleases tested. Likewise, for K562 cells, cssDNA displayed higher HDR rates than T-lssDNA molecules for all the nucleases tested, although collectively it did not achieve statistical significance.

HDR efficiency provides another metric for describing editing outcomes, where the fraction of total editing [GFP/(GFP+mCherry)] is the ''HDR ratio.'' The HDR efficiency of SpyCas9 and different Cas12a nucleases displayed cell-line-specific differences. In HEK293T cells, all three Cas12a variants yielded higher HDR ratios relative to SpyCas9 with both donors (Supplementary Fig. 5C). SpyCas9 yielded HDR efficiencies of 18% and 9.5% with cssDNA and T-lssDNA donors, respectively (Fig. 2A, lower panel). Cas12a orthologs increased HDR efficiencies to 25–31% with the cssDNA template and to 12–21% with the lssDNA donor. In K562 cells, LbaCas12a and FnoCas12a again yielded higher HDR ratios relative to SpyCas9 with both donors (Supplementary Fig. 5C).

However, AspCas12a yielded similar or lower HDR ratios relative to SpyCas9 with both donors. These trends hold for the bulk HDR rates, with LbaCas12a and FnoCas12a being superior to SpyCas9, and AspCas12a being similar or worse than SpyCas9. Notably, the HDR ratio for the Cas12a variants with cssDNA was 0.5–0.8 across both the cell lines (Supplementary Fig. S5C). Thus, the HDR pathway was being efficiently harnessed for DSB repair during Cas12a-mediated genome editing with the cssDNA donor. Taken together, these results indicate that Cas12a orthologs may be superior for template-dependent HDR genome editing when compared with SpyCas9, in particular when using a cssDNA donor.

The effect of donor orientation is dependent on cell type and nuclease identity

There are conflicting reports in the literature regarding the effect of DNA strand orientation on HDR efficiencies. A bias in HDR efficiency toward ssDNA donors that have the same sequence as the target strand (i.e., the strand base paired to the SpyCas9 RNA guide) has been reported.[17,69] However, others have not observed a

significant effect of strand orientation on HDR efficiency.[13,68,70] To examine strand-specific donor bias in HDR efficiencies in TLR-MCV1 cells, we generated target-strand-complementary (sense) and nontarget-strand-complementary (antisense) ssDNA donors for both linear and circular DNAs and electroporated them along with SpyCas9 and AspCas12a RNPs. For both effectors, the guide RNA was complementary to the antisense strand of the reporter, TLR-MCV1.

In K562-TLR-MCV1 cells, there were no significant differences between sense and antisense ssDNA donors except in the case of AspCas12a and cssDNA donors (Fig. 2B and Supplementary Fig. S5D). For AspCas12a with cssDNA, there was about a twofold increase in HDR efficiency with the sense donor relative to the antisense donor. In HEK293T-TLR-MCV1 cells, sense cssDNA donors produced significantly higher HDR yields than antisense cssDNA donors with both SpyCas9 and AspCas12a. The increase in the HDR efficiency with sense cssDNA relative to antisense cssDNA was 7% and 13% when cells were electroporated with SpyCas9 and AspCas12a, respectively. No significant difference was observed between the different lssDNA strands with either nuclease.

To examine if the two different guide orientations relative to the coding region of the TLR-MCV1 sequence influence the ssDNA donor orientation preference for HDR for SpyCas9 in K562 cells, we electroporated cssDNA and lssDNA donors that were complementary to the TLR-MCV1 sense or the antisense strand in combination with guide RNAs that were likewise complementary to either TLR-MCV1 target site strand (Supplementary Fig. S6A). We did not observe any significant differences in HDR efficiency as a function of relative guide/donor strand orientation (Supplementary Fig. S6B). Overall, while there are nuclease- and cell-type-specific differences in HDR efficiencies, the relative orientation of the donor does not have a consistent impact on HDR-based editing. This is consistent with previously described ssDNA donor strand biases in HDR efficiencies, which are generally locus- and cell-type specific.[18]

cssDNA donors are more potent than lssDNA donors for HDR

We reasoned that the higher nuclease stability of cssDNA donors may improve the potency of cssDNA compared with lssDNA donors. To test this hypothesis, cells were electroporated with increasing amounts of ssDNA donors while keeping the amount of SpyCas9 or AspCas12a RNPs constant (Fig. 2C). In K562 cells, the HDR yields peaked around 1–1.2 pmol of cssDNA for both SpyCas9 and AspCas12a. We also observe severe apparent DNA toxicity at higher donor DNA concentrations (>1.25 pmoles of cssDNA) resulting in reduction of HDR efficiencies.

Since cssDNA templates are about four to five times longer than their lssDNA counterparts due to the presence of the phagemid sequence elements, it is likely that DNA toxicity is associated with the total mass of DNA delivered instead of moles of DNA templates electroporated. Even so, the lssDNA donor did not perform as well as the cssDNA donor in stimulating HDR even at the highest concentration that was tested in K562 cells. The highest HDR efficiency observed for the lssDNA was about 5% with SpyCas9 and 7% with AspCas12a, which is four and two times lower than what was achieved with the cssDNA donor and SpyCas9 and AspCas12a, respectively.

In HEK293T cells, the cssDNA donor was more potent in stimulating GFP integration compared with the lssDNA donor (Fig. 2C). AspCas12a potentiated higher HDR efficiencies compared with SpyCas9 in HEK293T cells when used in conjunction with both lssDNA and cssDNA. Twenty-five percent HDR efficiency was observed for two pmols of cssDNA when codelivered with AspCas12a, whereas 5 pmols of cssDNA was needed to achieve similar integration efficiency with SpyCas9.

Integration efficiencies for lssDNA observed with both AspCas12a and SpyCas9 were at least twofold lower than those observed for comparable amounts of cssDNA. However, 20 pmoles of lssDNA was able to achieve 30% integration efficiency with AspCas12a, but this required fivefold more DNA than the amount of cssDNA donor needed to achieve comparable integration efficiency. Hence, cssDNA is more potent than lssDNA for HDR and its effect is further enhanced when using AspCas12a as the nuclease. Collectively, the TLR-MCV1-based experiments reveal that the cssDNA donors are more efficient at promoting HDR compared with the lssDNA donors.

cssDNA donors provide efficient templates for fluorescent tagging of endogenous proteins

For many functional genomic studies and gene therapy applications, targeted insertion of long DNA cassettes into endogenous loci is desirable. Most studies aimed at making targeted insertions of long DNA cassettes use plasmid donors to provide the template for precise insertion.[8] However, plasmid donors can be toxic to target cells, which makes insertion of long DNA cassettes an inefficient process in most cell types.[14] To test the suitability of cssDNA for integrating larger inserts, we chose four endogenous genes in the mammalian genome based on the work of Roberts et al[8] and He et al[71] to make targeted

insertions of fluorescent proteins (Fig. 3A). SpyCas9 RNPs were complexed with chemically synthesized guide-RNAs (listed in Supplementary Table S3) with terminal modifications to enhance intracellular stability.

Electroporation of RNPs in the absence of donor DNA into HEK293T cells yielded 80–93% indels at the four sites as measured by TIDE analysis (Supplementary Fig. S7),[34] indicating efficient SpyCas9 editing of each endogenous locus. It should be noted that while guides targeting *ACTB*, *TOMM20*, and *GAPDH* loci are complementary to the sense strand, the guide targeting *SEC61B* is complementary to the antisense strand. To evaluate the relative efficiency of targeted insertion by cssDNA and lssDNA, we tagged three endogenous open reading frames (*SEC61B*, *TOMM20*, and *ACTB*) through a direct fusion of mEGFP (Fig. 3A). At the *GAPDH* locus, we inserted an internal ribosome entry site-enhanced green fluorescence protein (EGFP) cassette to facilitate separate expression of both gene products from the modified locus.[71]

To evaluate the impact of the donor cassette sequence composition on HDR efficiency, the GFP tag was replaced with a red fluorescent tag (dTomato/iTag RFP) in a corresponding donor set. Phagemid-derived cssDNA or T-lssDNA donors encoding the fluorescent tag flanked by 1 kb homology arms were electroporated into K562 and HEK293T cells along with SpyCas9 RNPs, after which GFP- or red fluorescent protein (RFP)-positive cells were measured by flow cytometry to estimate the HDR-based recoding efficiency at each site of interest.

Collectively at all the loci tested, cssDNA resulted in a significantly higher frequency of functional tag integration compared with the linear T-lssDNA (Fig. 3B–E; significance values computed in Supplementary Table S5). Interestingly, although GFP, iTagRFP, and dTomato fusion tags have coding sequences of similar length, we observed higher integration efficiency with the GFP cssDNA donor at the *ACTB* and *TOMM20* locus, especially in HEK293T cells, indicating that donor cassette composition may modestly influence integration efficiency in a cell-type- and locus-specific manner. Similarly, at the *SEC61B* locus, cssDNA-mediated integration of the dTomato tag was higher than what was achieved with T-ssDNA in both the K562 cells and HEK293T cells (Fig. 3D). As expected, we did not observe substantial differences in donor integration efficiencies between T-lssDNA and B-lssDNA donors, although variability in the efficacy was observed depending on the target site, donor composition, and cell type (Supplementary Fig. S8).

As with TLR-MCV1, we observed cell-type- and site-specific differences in editing efficiencies with different cssDNA donor orientations, but there was no consistent trend that defined a preferred combination of target site and donor template strand (Supplementary Fig. S9). Collectively, while we observe cell-type-, locus-, and donor DNA sequence-, and orientation-dependent variability in DNA integration efficiencies, our results show the increased potency of cssDNA templates for tagging proteins at various endogenous genomic loci in comparison with lssDNA templates.

cssDNA can effectively drive biallelic tagging of endogenous proteins

Biallelic tagging of a target gene is often desirable for functional genomic studies, but this outcome is often hampered by a low HDR efficiency. Since we observed high yields of integration with cssDNA in both the tested cell lines, we reasoned that cssDNA would be able to support biallelic tagging. To distinguish between monoallelic and multiallelic integration, we electroporated equimolar amounts of cssDNA donors containing green and red fluorescent tags along with the appropriate SpyCas9 RNP into cells and measured fluorescence in these cells using flow cytometry. The majority of labeled cells expressed a single green or red fluorescent tag (Fig. 4). Encouragingly, for *ACTB*, *TOMM20*, and *SEC61B* loci, 17–26% of fluorescent cells were tagged with both the GFP and RFP, indicating integration of both the reporter tags at these sites (Supplementary Fig. S10).

Since our detection approach relies only on detection of the red and green fluorescence signals coming from the tagged gene, it is difficult to distinguish between biallelic and multiallelic tagging in HEK293T and K562 cells since these cell lines have been described as hypotriploid and triploid, respectively (ATCC CRL-3216, ATCC-CCL-243). Negligible levels of biallelic integration were observed at the *GAPDH* locus, likely due to the lower overall HDR efficiencies at this locus, which could reflect toxicity associated with tagging glyceraldehyde 3-phophate dehydrogenase (GAPDH), an essential housekeeping protein.

To further compare the efficiency of fluorescent tag integration at the genetic loci of interest using cssDNA and lssDNA, we set up a competition assay and tested different combinations of cssDNA and lssDNA donors for their abilities to insert reporter tags at the *ACTB* locus (Fig. 4B). We observed robust biallelic tagging when cssDNA donors encoding GFP and iTAG-RFP tags were cotransfected in both HEK293T cells (Fig. 4B) and K562 cells (Supplementary Fig. S11). Interestingly, when cssDNA was combined with an equimolar quantity of lssDNA to perform the knockins, we observed a 30-fold higher RFP signal over the GFP signal when RFP-encoding cssDNA was cointroduced with GFP-encoding lssDNA. Conversely, the combination of

GFP-encoding cssDNA with RFP-encoding lssDNA yielded 10-fold more GFP-positive than RFP-positive cells (Fig. 4B).

Overall, these results confirm that cssDNA is more efficient than lssDNA as an HDR donor in cultured human cells and is effective for generating biallelic insertions of extended coding sequences into the genome.

Discussion

For most cellular applications, nonviral methods for the delivery of a donor DNA template are used to achieve targeted DNA insertion at a locus of interest, owing to the ease of template production. Most previous nonviral approaches have used oligonucleotides, plasmids, or linear dsDNAs as the donor DNA template.[8,16,72–74] Long lssDNA templates have been demonstrated to provide advantages over dsDNA by both reducing toxicity to cells and increasing HDR efficiency of the DNA donor cassette.[22,23,27] More recently, long ssDNA molecules folded as compact nanostructures were used as templates for potentiating CRISPR-mediated HDR, providing an additional avenue for DNA compaction and delivery.[28] Enzymatic methods adopted for generating long ssDNAs have permitted the knockin of gene segments such as fluorescent reporter tags, which are more difficult to generate as chemically synthesized donors. However, cost-effective enzymatic synthesis of long ssDNA can be challenging.

In this study, we performed a side-by-side comparison of cssDNA produced from phagemids with lssDNA produced either using published protocols[23] or a biotin–streptavidin capture method that we adapted (Table 1).[33,49,75] The biotin-affinity approach for making lssDNA permits the efficient synthesis of longer DNA templates and is not subject to the potential fidelity issues of RT-based approaches, as the lssDNA is generated entirely by high-fidelity DNA polymerases. Overall, we found that phagemid-derived cssDNA, when codelivered with Cas9 or Cas12a RNPs, is highly effective in achieving targeted integration of DNA cassettes in mammalian cells. The production of cssDNA templates using phagemids is time- and cost-effective in comparison with methods for generating lssDNA donors, in part, because it requires fewer electrophoretic or affinity purification steps.

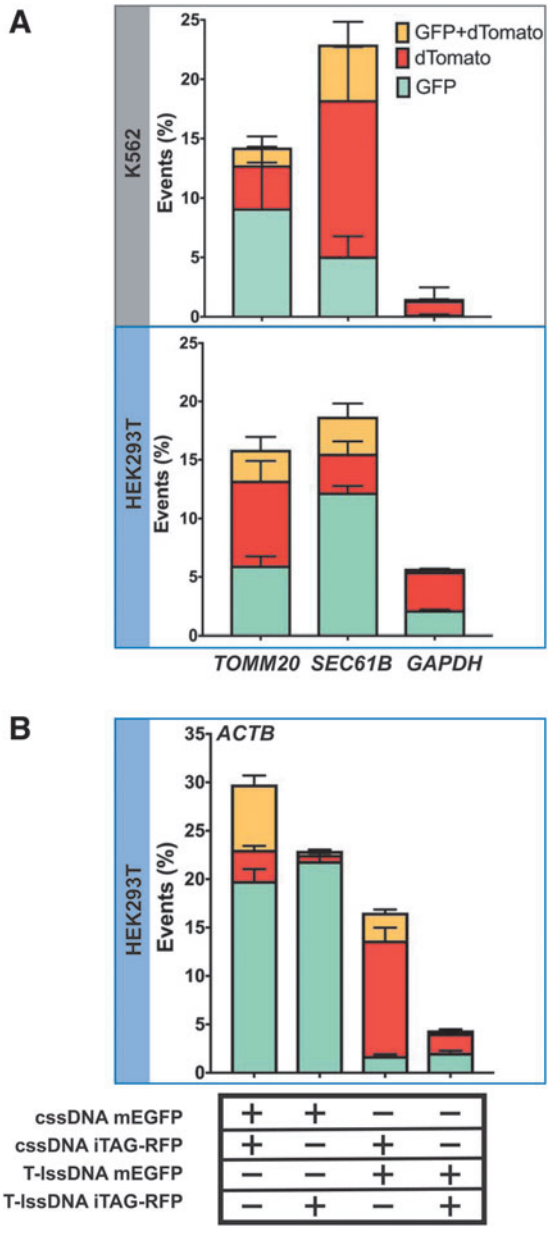

FIG. 4. Biallelic tagging of endogenous proteins using two different cssDNA donor templates. **(A)** The graphs show the percentage of fluorescent cells tagged with GFP (shown in cyan), dTomato (shown in red), or both (shown in yellow) at each locus (*TOMM20*, *SEC61B*, or *GAPDH*) in K562 cells (top panel) and HEK293T cells (bottom panel). Twenty picomole of SpyCas9 RNPs were codelivered with 0.5 pmol of each cssDNA template. Bars represent the mean from three independent biological replicates and error bars represent s.e.m. **(B)** Competition between cssDNA and lssDNA templates as donors for HDR. The graph shows the percentage of cells tagged with GFP (shown in cyan), iTAG-RFP (shown in red), or both GFP and iTAG-RFP (shown in yellow) at the *ACTB* locus. Bars represent the mean from three independent biological replicates and error bars represent s.e.m.

We examined the relative efficacy of HDR potentiated by different ssDNA donor compositions in the context of different Cas nuclease effectors, relative strand orientations, and donor doses. We initially assessed the effects of these parameters and the donor compositions on HDR efficiencies using a modified TLR system (TLR-MCV1). This fluorescence-based system permits simultaneous evaluation of imprecise and HDR-based editing efficiencies with a range of Cas9 and Cas12a effectors. While we observed robust integration of the GFP correction cassette using SpyCas9, Cas12a nucleases achieved higher overall yields of donor integration. The effects of ssDNA orientation, whether lssDNA or cssDNA, exhibited cell-line- and target-site-specific variability.

Overall, the potency of cssDNA donors was significantly higher (i.e., effective at lower doses) than lssDNA donors, with the reporter, TLR-MCV1, as well as at endogenous sites. When used in conjunction with SpyCas9 RNP, cssDNA-based HDR was robust even at concentrations as low as 1 pmol cssDNA donor per 100,000 cells, while lssDNA donors were 2- to 10-fold less effective at this dose. The use of large amounts of donor DNA to drive longer insertions in cell lines typically poses toxicity issues. The improved HDR potencies of cssDNA donors relative to those of the corresponding lssDNAs could arise from higher stability of these templates in cells since the circular topology likely confers some resistance to exonucleases. Consistent with this hypothesis, post-synthetic circularization of an lssDNA template increased the HDR efficiency by about twofold in K562 cells to levels that were comparable with phagemid-sourced cssDNA.

In addition to exonuclease resistance conferred by circular topology, phagemid-derived ssDNA templates offer several other advantages over lssDNA templates generated using RT- or PCR-based approaches:

(1) cssDNA can be generated with longer donor cassettes.[76] Excluding the encoded bacterial and phage DNA sequences (~2200 bp), our experience indicates that DNA cassettes up to ~10 kb can be readily incorporated into the phagemid vector for successful ssDNA generation (Supplementary Fig. S12), without any concomitant increase in generation cost or production of truncated products. While lssDNA has the advantage of only containing the sequence of interest, creating donors of this length would be extremely challenging with TGIRT and potentially cumbersome even for PCR-based approaches.

(2) TGIRT does not possess proofreading activity, and therefore, the fidelity of ssDNA products that it produces is of concern, especially for longer donors. By contrast, the biotin–streptavidin affinity purification-based approach for generation of lssDNA and phagemid-derived cssDNA described in this article can be used to generate accurate and full-length ssDNA.

(3) The cost of generating full-length cssDNA molecules is modest compared with lssDNA generation by RT-based methods or the biotin–streptavidin affinity purification approach, which use expensive enzymes and DNA purification kits (Table 1). Moreover, the production of cssDNA can be readily scaled up to generate several micrograms of DNA at a relatively low cost, which would be cumbersome to accomplish using *in vitro* approaches. Overall, the efficacy of phagemid-derived cssDNAs as HDR templates, combined with their ease and economy of production, make them an attractive alternative for precise genome editing. cssDNA templates should prove advantageous for the efficient insertion of long DNA cassettes in a variety of different cell types and can be leveraged for basic science and potentially stem cell-based therapeutic applications.

Acknowledgment

All new reagents described in this work have been deposited with the nonprofit plasmid-distribution service Addgene.

Authors' Contributions

E.J.S., P.D.Z., C.P.E., and S.A.W. directed the study. S.I., A.M., E.J.S., and S.A.W. conceived the study. S.I., A.M., J.V.-B., B.P.R., R.I., J.L., P.L., E.M., D.G., and J.S.B. performed the experiments. L.J.Z. performed the statistical analysis of data. S.I., A.M., E.J.S., and S.A.W. analyzed the data. S.I., A.M., E.J.S., and S.A.W. wrote the article with contributions from all the authors.

Author Disclosure Statement

No competing financial interests exist.

Funding Information

This work was supported by the U.S. National Institutes of Health grants (1R01GM115911, Somatic Cell Genome Editing grant UG3TR002668, and 4D Nucleome Grant U54DK107980) to Erik J. Sontheimer and Scot A. Wolfe, and the NIH grant F31DK120333 to Raed Ibraheim.

Supplementary Material

Supplementary Figure S1
Supplementary Figure S2
Supplementary Figure S3
Supplementary Figure S4
Supplementary Figure S5
Supplementary Figure S6
Supplementary Figure S7
Supplementary Figure S8
Supplementary Figure S9
Supplementary Figure S10

Supplementary Figure S11
Supplementary Figure S12
Supplementary Table S1
Supplementary Table S2
Supplementary Table S3
Supplementary Table S4
Supplementary Table S5

References

1. Anzalone AV, Koblan LW, Liu DR. Genome editing with CRISPR-Cas nucleases, base editors, transposases and prime editors. Nat Biotechnol 2020;38(7):824–844; doi: 10.1038/s41587-020-0561-9.
2. Wu WY, Lebbink JHG, Kanaar R, et al. Genome editing by natural and engineered CRISPR-associated nucleases. Nat Chem Biol 2018;14(7):642–651; doi: 10.1038/s41589-018-0080-x.
3. Vriend LE, Krawczyk PM. Nick-initiated homologous recombination: Protecting the genome, one strand at a time. DNA Repair (Amst) 2017;50(1–13); doi: 10.1016/j.dnarep.2016.12.005.
4. Porteus MH, Baltimore D. Chimeric nucleases stimulate gene targeting in human cells. Science 2003;300(5620):763; doi: 10.1126/science.1078395.
5. Rothkamm K, Kruger I, Thompson LH, et al. Pathways of DNA double-strand break repair during the mammalian cell cycle. Mol Cell Biol 2003;23(16):5706–5715; doi: 10.1128/mcb.23.16.5706–5715.2003.
6. Sander JD, Joung JK. CRISPR-Cas systems for editing, regulating and targeting genomes. Nat Biotechnol 2014;32(4):347–355; doi: 10.1038/nbt.2842.
7. Richardson CD, Kazane KR, Feng SJ, et al. CRISPR-Cas9 genome editing in human cells occurs via the Fanconi anemia pathway. Nat Genet 2018;50(8):1132–1139; doi: 10.1038/s41588-018-0174-0.
8. Roberts B, Haupt A, Tucker A, et al. Systematic gene tagging using CRISPR/Cas9 in human stem cells to illuminate cell organization. Mol Biol Cell 2017;28(21):2854–2874; doi: 10.1091/mbc.E17-03-0209.
9. Yin H, Xue W, Chen S, et al. Genome editing with Cas9 in adult mice corrects a disease mutation and phenotype. Nat Biotechnol 2014;32(6):551–553; doi: 10.1038/nbt.2884.
10. Dever DP, Bak RO, Reinisch A, et al. CRISPR/Cas9 beta-globin gene targeting in human haematopoietic stem cells. Nature 2016;539(7629):384–389; doi: 10.1038/nature20134.
11. Schwank G, Koo BK, Sasselli V, et al. Functional repair of CFTR by CRISPR/Cas9 in intestinal stem cell organoids of cystic fibrosis patients. Cell Stem Cell 2013;13(6):653–658; doi: 10.1016/j.stem.2013.11.002.
12. Bak RO, Dever DP, Reinisch A, et al. Multiplexed genetic engineering of human hematopoietic stem and progenitor cells using CRISPR/Cas9 and AAV6. Elife 2017;6:e27873; doi: 10.7554/eLife.27873.
13. Liang X, Potter J, Kumar S, et al. Enhanced CRISPR/Cas9-mediated precise genome editing by improved design and delivery of gRNA, Cas9 nuclease, and donor DNA. J Biotechnol 2017;241:136–146; doi: 10.1016/j.jbiotec.2016.11.011.
14. Gaj T, Staahl BT, Rodrigues GMC, et al. Targeted gene knock-in by homology-directed genome editing using Cas9 ribonucleoprotein and AAV donor delivery. Nucleic Acids Res 2017;45(11):e98; doi: 10.1093/nar/gkx154.
15. Wang Y, Wang Y, Chang T, et al. Integration-defective lentiviral vector mediates efficient gene editing through homology-directed repair in human embryonic stem cells. Nucleic Acids Res 2017;45(5):e29; doi: 10.1093/nar/gkw1057.
16. Roth TL, Puig-Saus C, Yu R, et al. Reprogramming human T cell function and specificity with non-viral genome targeting. Nature 2018;559(7714):405–409; doi: 10.1038/s41586-018-0326-5.
17. Richardson CD, Ray GJ, DeWitt MA, et al. Enhancing homology-directed genome editing by catalytically active and inactive CRISPR-Cas9 using asymmetric donor DNA. Nat Biotechnol 2016;34(3):339–344; doi: 10.1038/nbt.3481.
18. Kan Y, Ruis B, Takasugi T, et al. Mechanisms of precise genome editing using oligonucleotide donors. Genome Res 2017;27(7):1099–1111; doi: 10.1101/gr.214775.116.
19. Schubert MS, Thommandru B, Woodley J, et al. Optimized design parameters for CRISPR Cas9 and Cas12a homology-directed repair. Sci Rep 2021;11(1):19482; doi: 10.1038/s41598-021-98965-y.
20. Ghanta KS, Chen Z, Mir A, et al. 5′-Modifications improve potency and efficacy of DNA donors for precision genome editing. Elife 2021;10:e72216; doi: 10.7554/eLife.72216.
21. Chen F, Pruett-Miller SM, Huang Y, et al. High-frequency genome editing using ssDNA oligonucleotides with zinc-finger nucleases. Nat Methods 2011;8(9):753–755; doi: 10.1038/nmeth.1653.
22. Quadros RM, Miura H, Harms DW, et al. Easi-CRISPR: A robust method for one-step generation of mice carrying conditional and insertion alleles using long ssDNA donors and CRISPR ribonucleoproteins. Genome Biol 2017;18(1):92; doi: 10.1186/s13059-017-1220-4.
23. Li H, Beckman KA, Pessino V, et al. Design and specificity of long ssDNA donors for CRISPR-based knock-in. bioRxiv 2017;2017:178905; doi: 10.1101/178905.
24. Bai H, Liu L, An K, et al. CRISPR/Cas9-mediated precise genome modification by a long ssDNA template in zebrafish. BMC Genomics 2020;21(1):67; doi: 10.1186/s12864-020-6493-4.
25. Yoshimi K, Kunihiro Y, Kaneko T, et al. ssODN-mediated knock-in with CRISPR-Cas for large genomic regions in zygotes. Nat Commun 2016;7:10431; doi: 10.1038/ncomms10431.
26. Minev D, Guerra R, Kishi JY, et al. Rapid in vitro production of single-stranded DNA. Nucleic Acids Res 2019;47(22):11956–11962; doi: 10.1093/nar/gkz998.
27. Miura H, Quadros RM, Gurumurthy CB, et al. Easi-CRISPR for creating knock-in and conditional knockout mouse models using long ssDNA donors. Nat Protoc 2018;13(1):195–215; doi: 10.1038/nprot.2017.153.
28. Lin-Shiao E, Pfeifer WG, Shy BR, et al. CRISPR-Cas9-mediated nuclear transport and genomic integration of nanostructured genes in human primary cells. Nucleic Acids Res 2022;50(3):1256–1268; doi: 10.1093/nar/gkac049.
29. Kunkel TA. Rapid and efficient site-specific mutagenesis without phenotypic selection. Proc Natl Acad Sci U S A 1985;82(2):488–492; doi: 10.1073/pnas.82.2.488.
30. Lin C, Rinker S, Wang X, et al. In vivo cloning of artificial DNA nanostructures. Proc Natl Acad Sci U S A 2008;105(46):17626–17631; doi: 10.1073/pnas.0805416105.
31. Smith GP. Filamentous fusion phage: Novel expression vectors that display cloned antigens on the virion surface. Science 1985;228(4705):1315–1317; doi: 10.1126/science.4001944.
32. Iyer S, Doktycz MJ. Thrombin-mediated transcriptional regulation using DNA aptamers in DNA-based cell-free protein synthesis. ACS Synth Biol 2014;3(6):340–346; doi: 10.1021/sb4000756.
33. Mitchell LG, Merril CR. Affinity generation of single-stranded DNA for dideoxy sequencing following the polymerase chain reaction. Anal Biochem 1989;178(2):239–242; doi: 10.1016/0003-2697(89)90631-3.
34. Brinkman EK, Chen T, Amendola M, et al. Easy quantitative assessment of genome editing by sequence trace decomposition. Nucleic Acids Res 2014;42(22):e168; doi: 10.1093/nar/gku936.
35. Iyer S, Suresh S, Guo D, et al. Precise therapeutic gene correction by a simple nuclease-induced double-stranded break. Nature 2019;568(7753):561–565; doi: 10.1038/s41586-019-1076-8.
36. Xu S, Luk K, Yao Q, et al. Editing aberrant splice sites efficiently restores beta-globin expression in beta-thalassemia. Blood 2019;133(21):2255–2262; doi: 10.1182/blood-2019-01-895094.
37. Liu P, Luk K, Shin M, et al. Enhanced Cas12a editing in mammalian cells and zebrafish. Nucleic Acids Res 2019;47(8):4169–4180; doi: 10.1093/nar/gkz184.
38. Wu Y, Zeng J, Roscoe BP, et al. Highly efficient therapeutic gene editing of human hematopoietic stem cells. Nat Med 2019;25(5):776–783; doi: 10.1038/s41591-019-0401-y.
39. Ihaka R, Gentleman R. R: A language for data analysis and graphics. J Comput Graph Stat 1996;5(3):299–314; doi: 10.2307/1390807.
40. Lenth RV. Least-squares means: The R package lsmeans. J Comput Graph Stat 2016;69(1):33; doi: 10.18637/jss.v069.i01.
41. Huang Y, Hsu JC. Hochberg's step-up method: Cutting corners off Holm's step-down method. Biometrika 2007;94(4):965–975; doi: 10.1093/biomet/asm67.
42. Qi H, Lu H, Qiu HJ, et al. Phagemid vectors for phage display: Properties, characteristics and construction. J Mol Biol 2012;417(3):129–143; doi: 10.1016/j.jmb.2012.01.038.
43. Zhou B, Dong Q, Ma R, et al. Rapid isolation of highly pure single-stranded DNA from phagemids. Anal Biochem 2009;389(2):177–179; doi: 10.1016/j.ab.2009.03.044.

44. Vieira J, Messing J. Production of single-stranded plasmid DNA. Methods Enzymol 1987;153:3–11; doi: 10.1016/0076–6879(87)53044-0.
45. Miura H, Gurumurthy CB, Sato T, et al. CRISPR/Cas9-based generation of knockdown mice by intronic insertion of artificial microRNA using longer single-stranded DNA. Sci Rep 2015;5:12799; doi: 10.1038/srep12799.
46. Leonetti MD, Sekine S, Kamiyama D, et al. A scalable strategy for high-throughput GFP tagging of endogenous human proteins. Proc Natl Acad Sci U S A 2016;113(25):E3501–E3508; doi: 10.1073/pnas.1606731113.
47. Xiong Y, Eickbush TH. Origin and evolution of retroelements based upon their reverse transcriptase sequences. EMBO J 1990;9(10):3353–3362; doi: 10.1002/j.1460-2075.1990.tb07536.x.
48. Harrison GP, Mayo MS, Hunter E, et al. Pausing of reverse transcriptase on retroviral RNA templates is influenced by secondary structures both 5′ and 3′ of the catalytic site. Nucleic Acids Res 1998;26(14):3433–3442; doi: 10.1093/nar/26.14.3433.
49. Fu Y, Yang Y, Zhang H, et al. The genome of the Hi5 germ cell line from Trichoplusia ni, an agricultural pest and novel model for small RNA biology. Elife 2018;7:e31628; doi: 10.7554/eLife.31628.
50. Certo MT, Ryu BY, Annis JE, et al. Tracking genome engineering outcome at individual DNA breakpoints. Nat Methods 2011;8(8):671–676; doi: 10.1038/nmeth.1648.
51. Cong L, Ran FA, Cox D, et al. Multiplex genome engineering using CRISPR/Cas systems. Science 2013;339(6121):819–823; doi: 10.1126/science.1231143.
52. Jinek M, Chylinski K, Fonfara I, et al. A programmable dual-RNA-guided DNA endonuclease in adaptive bacterial immunity. Science 2012;337(6096):816–821; doi: 10.1126/science.1225829.
53. Hou Z, Zhang Y, Propson NE, et al. Efficient genome engineering in human pluripotent stem cells using Cas9 from Neisseria meningitidis. Proc Natl Acad Sci U S A 2013;110(39):15644–15649; doi: 10.1073/pnas.1313587110.
54. Esvelt KM, Mali P, Braff JL, et al. Orthogonal Cas9 proteins for RNA-guided gene regulation and editing. Nat Methods 2013;10(11):1116–1121; doi: 10.1038/nmeth.2681.
55. Edraki A, Mir A, Ibraheim R, et al. A compact, high-accuracy Cas9 with a dinucleotide PAM for in vivo genome editing. Mol Cell 2019;73(4):714–726.e4; doi: 10.1016/j.molcel.2018.12.003.
56. Fonfara I, Le Rhun A, Chylinski K, et al. Phylogeny of Cas9 determines functional exchangeability of dual-RNA and Cas9 among orthologous type II CRISPR-Cas systems. Nucleic Acids Res 2014;42(4):2577–2590; doi: 10.1093/nar/gkt1074.
57. Yamada M, Watanabe Y, Gootenberg JS, et al. Crystal structure of the minimal Cas9 from *Campylobacter jejuni* reveals the molecular diversity in the CRISPR-Cas9 systems. Mol Cell 2017;65(6):1109–1121 e3; doi: 10.1016/j.molcel.2017.02.007.
58. Kim E, Koo T, Park SW, et al. In vivo genome editing with a small Cas9 orthologue derived from *Campylobacter jejuni*. Nat Commun 2017;8:14500; doi: 10.1038/ncomms14500.
59. Ran FA, Cong L, Yan WX, et al. In vivo genome editing using *Staphylococcus aureus* Cas9. Nature 2015;520(7546):186–191; doi: 10.1038/nature14299.
60. Harrington LB, Paez-Espino D, Staahl BT, et al. A thermostable Cas9 with increased lifetime in human plasma. Nat Commun 2017;8(1):1424; doi: 10.1038/s41467-017-01408-4.
61. Zetsche B, Gootenberg JS, Abudayyeh OO, et al. Cpf1 is a single RNA-guided endonuclease of a class 2 CRISPR-Cas system. Cell 2015;163(3):759–771; doi: 10.1016/j.cell.2015.09.038.
62. Zetsche B, Heidenreich M, Mohanraju P, et al. Multiplex gene editing by CRISPR-Cpf1 using a single crRNA array. Nat Biotechnol 2017;35(1):31–34; doi: 10.1038/nbt.3737.
63. DeWitt MA, Magis W, Bray NL, et al. Selection-free genome editing of the sickle mutation in human adult hematopoietic stem/progenitor cells. Sci Transl Med 2016;8(360):360ra134; doi: 10.1126/scitranslmed.aaf9336.
64. Liang X, Potter J, Kumar S, et al. Rapid and highly efficient mammalian cell engineering via Cas9 protein transfection. J Biotechnol 2015;208:44–53; doi: 10.1016/j.jbiotec.2015.04.024.
65. Schumann K, Lin S, Boyer E, et al. Generation of knock-in primary human T cells using Cas9 ribonucleoproteins. Proc Natl Acad Sci U S A 2015;112(33):10437–10442; doi: 10.1073/pnas.1512503112.
66. Kim S, Kim D, Cho SW, et al. Highly efficient RNA-guided genome editing in human cells via delivery of purified Cas9 ribonucleoproteins. Genome Res 2014;24(6):1012–1019; doi: 10.1101/gr.171322.113.
67. Hendel A, Bak RO, Clark JT, et al. Chemically modified guide RNAs enhance CRISPR-Cas genome editing in human primary cells. Nat Biotechnol 2015;33(9):985–989; doi: 10.1038/nbt.3290.
68. Wang Y, Liu KI, Sutrisnoh NB, et al. Systematic evaluation of CRISPR-Cas systems reveals design principles for genome editing in human cells. Genome Biol 2018;19(1):62; doi: 10.1186/s13059-018-1445-x.
69. Yang L, Guell M, Byrne S, et al. Optimization of scarless human stem cell genome editing. Nucleic Acids Res 2013;41(19):9049–9061; doi: 10.1093/nar/gkt555.
70. Lin S, Staahl BT, Alla RK, et al. Enhanced homology-directed human genome engineering by controlled timing of CRISPR/Cas9 delivery. Elife 2014;3:e04766; doi: 10.7554/eLife.04766.
71. He X, Tan C, Wang F, et al. Knock-in of large reporter genes in human cells via CRISPR/Cas9-induced homology-dependent and independent DNA repair. Nucleic Acids Res 2016;44(9):e85; doi: 10.1093/nar/gkw064.
72. Song F, Stieger K. Optimizing the DNA donor template for homology-directed repair of double-strand breaks. Mol Ther Nucleic Acids 2017;7:53–60; doi: 10.1016/j.omtn.2017.02.006.
73. Zhang Y, Zhang Z, Ge W. An efficient platform for generating somatic point mutations with germline transmission in the zebrafish by CRISPR/Cas9-mediated gene editing. J Biol Chem 2018;293(17):6611–6622; doi: 10.1074/jbc.RA117.001080.
74. Hayashi A, Tanaka K. Short-homology-mediated CRISPR/Cas9-based method for genome editing in fission yeast. G3 (Bethesda) 2019;9(4):1153–1163; doi: 10.1534/g3.118.200976.
75. Uhlen M. Magnetic separation of DNA. Nature 1989;340(6236):733–734; doi: 10.1038/340733a0.
76. Greenstein D, Brent R. Introduction to vectors derived from filamentous phages. Curr Protoc Mol Biol 2001;Chapter 1:Unit1 14; doi: 10.1002/0471142727.mb0114s13.

Received: June 5, 2022
Accepted: August 3, 2022
Online Publication Date: September 8, 2022